arXiv:1209.2253v1 [cond-mat.mes-hall] 11 Sep 2012

Spin-filtering and charge- and spin-switching effects in a quantum wire with periodically attached stubs

Xianbo Xiao,[1] Zhaoxia Chen,[2] Zhiming Rao,[1] Wenjie Nie[1] and Guanghui Zhou[3*]
[1]*School of Computer, Jiangxi University of Traditional Chinese Medicine, Nanchang 330004, China*
[2]*School of Mechatronics Engineering, East China Jiaotong University, Nanchang 330013, China and*
[3]*Department of Physics and Key Laboratory for Low-Dimensional Quantum Structures and Manipulation (Ministry of Education), Hunan Normal University, Changsha 410081, China*

Spin-dependent electron transport in a periodically stubbed quantum wire in the presence of Rashba spin-orbit interaction (SOI) is studied via the nonequilibrium Green's function method combined with the Landauer-Büttiker formalism. The coexistence of spin filtering, charge and spin switching are found in the considered system. The mechanism of these transport properties is revealed by analyzing the total charge density and spin-polarized density distributions in the stubbed quantum wire. Furthermore, periodic spin-density islands with high polarization are also found inside the stubs, owing to the interaction between the charge density islands and the Rashba SOI-induced effective magnetic field. The proposed nanostructure may be utilized to devise an all-electrical multifunctional spintronic device.

During the last decade, much effort has been made in using the electron spin in semiconductor to store and communicate information, often referred to as semiconductor spintronics.[1–3] The main challenge in this field is how to provide feasible methods to generate, manipulate, store, and detect spin-polarized electrons in semiconductor materials. The Rashba spin-orbit interaction (SOI),[4] which arises from the structural asymmetry of the confining potential in semiconductor quantum well, is regarded as a promising way. The practical advantage of the Rashba SOI is that its amplitude can be conveniently tuned by different means, including the ion distribution in the nearby doping layers,[5] the relative asymmetry of the electron density at the two quantum well interfaces,[6] and importantly, the applied voltage to surface gates.[7–9]

With the advances in modern nanotechnology, various kinds of high quality low-dimensional nanostructures and superlattice structures can be fabricated.[10] Recently, spin-dependent electron transport in nanostructures in the presence of Rashba SOI has drawn much attention for the purpose of application in spintronic devices. It is shown that the spin-dependent electron transport property is very sensitive to the geometrical structure symmetry of the considered system. For the two-terminal Rashba nanostructures with broken longitudinal symmetry such as zigzag wire,[11] electron stub waveguide,[12] and locally constricted electron waveguides,[13, 14] a spin-polarized current can be generated in the output lead. In addition, it has also been found that highly polarized spin-density islands can be formed inside nonuniform waveguides due to the structure-induced bound states.[12, 15] For the two-terminal transversally asymmetrical Rashba nanostructures, such as hornlike waveguide[16] and step-like quantum wire,[17] a very large spin conductance can be obtained when the forward bias is applied to the structures. However, it is suppressed strongly when the direction of bias is reversed.

Spin-dependent electron transport in superlattice structures has also been investigated extensively. A periodic and nearly square-wave pattern with wide gaps has been found in the transmission spectra of periodically stubbed electron waveguide with Rashba SOI for a spin-polarized injection, demonstrating the structure can be utilized to design a spin transistor.[18] Similarly, transmission gaps with a complete blocking of the charge current over a range of energy has been found in straight quantum wires under the modulation of spatially periodic Rashba SOI (electric field), which can be used as an ideal charge current switch.[19–25] Furthermore, ideal spin-filtering effect can also be achieved in straight quantum wires when they are modulated by spatially periodic Rashba SOI and magnetic field simultaneously.[26, 27] However, spin-dependent electron transport in periodic Rashba nanostructure with breaking of longitudinal symmetry in the case of spin-unpolarized injection, up to now, has not been studied yet.

In this letter, by means of nonequilibrium Green's function (GF) with tight-binding approximation scheme, we calculate the spin-dependent conductance and local spin-polarized density (LSPD) distribution for a periodically stubbed quantum wire in the presence of Rashba SOI. The quantum wire is sandwiched between two normal metal leads, as sketched in Fig. 1(a), with experimental setup proposal as shown in Fig. 1(b), where l_1 is the distance between nearest-neighbor

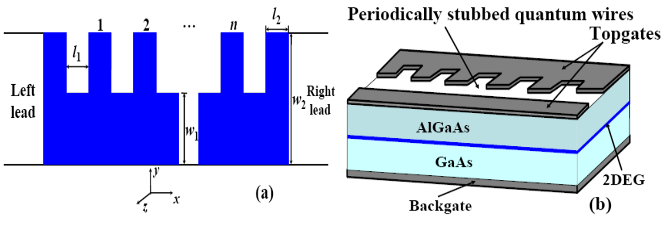

FIG. 1: (Color online) Schematic diagrams of (a) a periodically stubbed quantum wire with Rashba SOI and (b) the experimental setup proposal, where l_1 is the distance between nearest-neighbor stubs with length l_2 and width (w_2-w_1). The topgates produce the transverse confinement for the stubbed quantum wire while the backgate tunes the Rashba SOI strength.

---

[*] Electronic address: ghzhou@hunnu.edu.cn

stubs with constant length l_2 and width (w_2-w_1). The topgates produce the transverse confinement for the stubbed quantum wire while the backgate tunes the Rashba SOI strength. Interestingly, it is found that a spin-polarized current can be generated in the output lead, which is attributed to the asymmetrical distribution of spin-polarized density caused by the Rashba SOI in combination with the broken longitudinal symmetry of the system. Moreover, ideal charge and spin-polarized current switching effects are observed in the considered system, owing to minigaps in the energy band caused by the periodic stub structure. In addition, highly spin-polarized density islands have also been found inside stubs due to the interaction between the charge density islands and the Rashba SOI-induced effective magnetic field. Therefore, the proposed structure allows for practical applications, including spin filtering, charge and spin current switching, and spin storage.

Using the standard tight-binding formalism, the Hamiltonian for the considered system including Rashba SOI reads

$$\begin{aligned} H &= \sum_{lm\zeta} \varepsilon_{lm\zeta} c^{\dagger}_{lm\zeta} c_{lm\zeta} - t \sum_{lm\zeta} \{ c^{\dagger}_{l+1,m\zeta} c_{lm\zeta} + c^{\dagger}_{l,m+1,\zeta} c_{lm\zeta} + \text{H.c.} \} \\ &\quad - \gamma_R \sum_{lm\zeta\zeta'} \{ c^{\dagger}_{l+1,m,\zeta} c_{lm\zeta'} (i\sigma_y)^{\zeta\zeta'} - c^{\dagger}_{l,m+1,\zeta} c_{lm\zeta'} (i\sigma_x)^{\zeta\zeta'} + \text{H.c.} \} \\ &\quad + \sum_{lm\zeta} v_{lm\zeta} c^{\dagger}_{lm\zeta} c_{lm\zeta}, \end{aligned} \tag{1}$$

where $c^{\dagger}_{lm\zeta}(c_{lm\zeta})$ is the creation (annihilation) operator for an electron with spin $\zeta = \uparrow$ or $\downarrow$ on site (l, m), $\varepsilon_{lm\zeta} = 4t$ is the on-site energy with the electron hopping amplitude $t = \hbar^2/2m^* a^2$ (m^* and a are the effective mass of electron and lattice spacing, respectively), σ_x and σ_y are the Pauli matrixes, $\gamma_R = \alpha(2a)^{-1}$ is the Rashba SOI strength with the Rashba coefficient α, $v_{lm\zeta}$ is the additional confining potential, and H.c. means complex conjugate.

According to Hamiltonian (1), the outgoing wave amplitudes and the wave function of a scattered electron state can be obtained by adopting the spin-resolved recursive GF method.[12, 17] Then the two-terminal spin-dependent conductance is given by the Landauer-Büttiker formula[28, 29]

$$G^{\zeta\zeta'} = \frac{e^2}{h} \mathrm{Tr}(\Gamma^{\zeta}_{L} G^{\zeta\zeta'}_{r} \Gamma^{\zeta'}_{R} G^{\zeta'\zeta}_{a}), \tag{2}$$

in which $\Gamma_{L(R)}$ denotes the self-energy function for the isolated ideal leads, $G^{\zeta\zeta'}_{r}$ ($G^{\zeta'\zeta}_{a}$) is the retarded (advanced) GF of the whole structure, and Tr means the trace over the spatial and spin degrees of freedom. The total charge density distribution and the LSPD distribution of the z-component of electrons in the system are defined respectively as[12, 30]:

$$\rho^{total}(x, y) = \sum_{q,\zeta} \psi^{\dagger}_{q\zeta}(x, y) \psi_{q\zeta}(x, y), \tag{3}$$

and

$$LP_z(x, y) = \sum_{q,\zeta} \psi^{\dagger}_{q\zeta}(x, y) \sigma_z \psi_{q\zeta}(x, y), \tag{4}$$

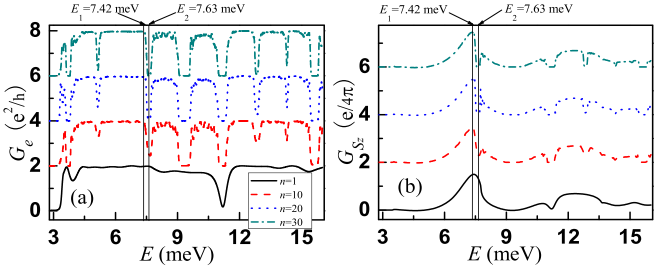

FIG. 2: (Color online) The calculated (a) charge conductance and (b) the z-component spin conductance spectra for the system with number of stubs n=1 (black) solid, 10 (red) dashed, 20 (blue) dotted and 30 (green) dash-dotted, where the graphs are vertically offset 2.0 for comparison.

where $\psi_{q\zeta}(x, y)$ is the velocity-normalized scattered wave function of an electron injected from the lead in the qth subband with spin $\zeta = \uparrow$ or $\downarrow$, and the summation is taken over all the propagating modes in the lead.

The z-axis is taken as the spin-quantized axis so that $|\uparrow\rangle = (1, 0)^{\mathrm{T}}$ represents the spin-up state and $|\downarrow\rangle = (0, 1)^{\mathrm{T}}$ denotes the spin-down state, where T means transposition. Therefore, the charge conductance and the spin conductance of z-component are accordingly defined as

$$G_e = G^{\uparrow\uparrow} + G^{\uparrow\downarrow} + G^{\downarrow\downarrow} + G^{\downarrow\uparrow} \tag{5}$$

and

$$G_{S_z} = \frac{e}{4\pi} \frac{G^{\uparrow\uparrow} + G^{\downarrow\uparrow} - G^{\downarrow\downarrow} - G^{\uparrow\downarrow}}{e^2/h}, \tag{6}$$

respectively.

In what follows, we present some numerical examples for the system. In the calculation the physical quantities are chosen to be that for a high-mobility GaAs/Al$_x$Ga$_{1-x}$ heterostructure[31] with a typical electron density $N \sim 2.5 \times 10^{11}/\mathrm{cm}^2$ and $m^* = 0.067 m_e$, where m_e is the mass of free electron. The periodically stubbed quantum wire is formed by adding top-gates upon the heterostructure, as shown in Fig. 1(b), with fixed geometrical structure parameters $l_1 = l_2 = 40$ nm, $w_1 = 36$ nm, and $w_2 = 80$ nm. The strength of the Rashba SOI can be controlled by a back-gate and the Rashba coefficient is set as $\alpha = 43.7$ meV·nm. For simplicity, the hard-wall potential approximation is chosen as the transverse confining potential and the lattice spacing is taken as $a = 4$ nm.

Figures 2(a) and 2(b) show the charge and spin conductances as function of the electron energy for various stub numbers, respectively. For the quantum wire with one stub only, the resonance and antiresonance structures are found in the charge conductance, as shown by the (black) solid line in Fig. 2(a), originating from the interference between the continue states in the wire and the quasi-bound states in the stub.[12] When the number of the stubs increases to n=10, minibands appear in the charge conductance spectrum as shown by the (red) dashed line. As the number of the stubs increases fur-

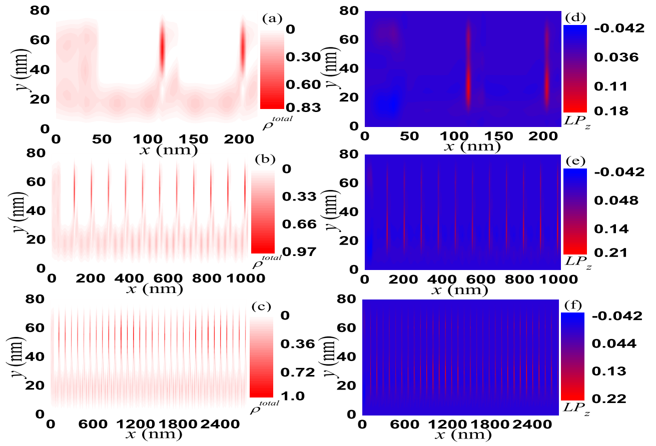

FIG. 3: (Color online) The total charge density (the left panels) and LSPD (the right panels) distributions in stubbed quantum wire with different length (different number of stubs), where the electron energy is taken as $E_1 = 7.42$ meV. The concerned density in all the panels are normalized against the highest value in (c).

ther, the charge conductance around the antiresonances decreases gradually and finally extends into minigaps [see the (blue) dotted and (green) dash-dotted lines in Fig. 2(a)]. The formation of the minibands and minigaps is attributed to that the period of the stubs on quantum wire $L = l_1 + l_2 = 80$ nm is much larger than the lattice spacing a=4 nm, which leads to the split of the energy band. This effect very resembles the result as found in a Rashba wire under the modulation of longitudinal periodic potential.[25] In addition, the charge conductance oscillations are also found in the allowed bands between the nearest two minigaps and they become more rapid with increasing stub numbers. The characteristics of the charge conductance described above is similar to that of a longitudinal symmetrical waveguide system with attached stubs.[32] However, the spin conductance exhibits very different behaviors, as shown in Fig. 2(b). For the quantum wire with single stub, a nonzero spin conductance can be obtained. Particularly, a broad spin conductance peak with very large magnitude emerges when the electron energy at E_1=7.42 meV. Interestingly, spin conductance minigaps appear with the increase of stub numbers and their positions are the same as that of the charge conductance minigaps. Unexpectedly, the broad peak happens to be split by a minigap. Moreover, the magnitude of the spin conductance in the allowed band almost keeps invariable except for the emergence of some small oscillations, demonstrating that the spin conductance is mainly determined by the longitudinal structures while has less relation with the number of stubs.

In order to further understand the behavior for charge and spin conductances in Fig. 2, the distributions of total charge density and LSPD for the system with different number of stubs are shown in Fig. 3. The electron energy is taken as E_1=7.42 meV, i.e., a value locates inside the broad peak of spin conductance but outside the minigap of charge conductance (see Fig. 2). For the quantum wire with single stub, as shown in Fig. 3(a), the total charge density distribution

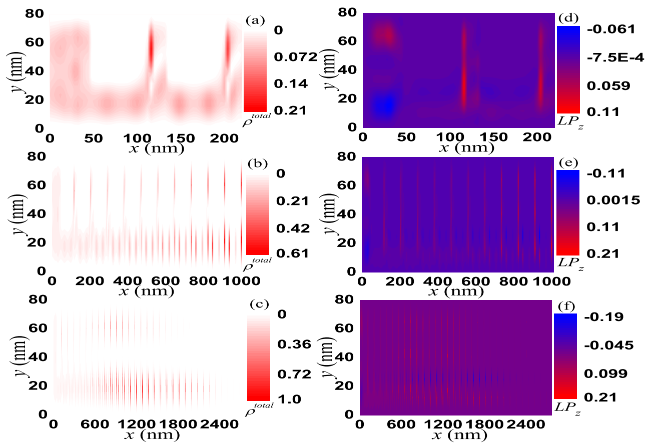

FIG. 4: (Color online) The same as Fig. 3 but the energy E_2=7.63 meV.

in the narrow regions and the left wide region displays regular stripes, which represent propagating modes. Interestingly, the lower propagating mode spreads along the whole system. However, the higher propagating mode is strongly localized in the system, that is, charge density islands are formed inside the stub and the right wide region. The former island results from the interference between the forward electron waves and the backward electron waves scattered by the corners, while the latter island originates from the interference between the forward electron waves and the backward electron waves scattered by the wire-lead interface.[17] When the number of the stubs is increased, as demonstrated in Fig. 3(b) and 3(c), periodic charge density islands are formed in the stubs and their magnitudes are slightly enhanced. Meanwhile, the lower propagating mode still spreads along the whole wire, leading to the unchangeableness of the charge conductance at this position [see Fig. 2(a)]. Figure 3(d) plots the LSPD distribution LP_z for electrons in the quantum wire with single stub. Interestingly, highly spin-polarized density islands are formed inside the stub and the right wide region, owing to the interaction between the charge density islands and the Rashba SOI-induced effective magnetic fields.[12, 15] Further, only spin-polarized density islands with positive sign are generated inside the stubs because of the longitudinal asymmetry of the considered system. As a result, a spin conductance with positive sign can be achieved at this electron energy [see Fig. 2(b)]. In addition, similar to the behaviors of the total charge density distribution in Figs. 3(b) and 3(c), periodic spin-polarized density islands arise in the stubs and their magnitudes strengthened slightly in some places, as shown in Figs. 3(e) and 3(f), with the increase of stub numbers. Therefore, the spin conductance within the allowed band nearly keeps a constant.

Figure 4 shows the total charge density and LSPD distributions of electrons in the stubbed quantum wire for another energy $E_2 = 7.63$ meV, a value inside both the broad peak and minigap as seen in Fig. 2. For the quantum wire attached a single stub, as shown in Fig. 4(a), the salient characters of the total charge density distribution are the same as those in

Fig. 3(a). However, the behaviors of the total charge density distribution for the quantum wire connected to periodic stubs, as shown in Figs. 4(b) and 4(c), are very different from that in Figs. 3(b) and 3(c). Apart from the charge density islands formed inside the stubs, charge density islands are also formed in the narrow regions of the quantum wire with the increasing number of stubs. Furthermore, the magnitudes of the charge density islands are increased dramatically. Finally, the lower propagating mode is also completely localized in the system, as shown in Fig. 4(c). Consequently, the charge conductance decreases gradually and reach zero at final, as seen in Fig. 2(a), with raising stub numbers. Similarly, the characteristics of the LSPD distribution for the singly stubbed quantum wires, as depicted in Fig. 4(d), are the same as that in Fig. 3(d). However, for the quantum wires with periodic stubs, highly spin-polarized density islands with negative sign emerge in the narrow areas of the quantum wire besides those inside the stubs with positive sign, as shown in Figs. 4(e) and 4(f). Moreover, the magnitudes of the spin-polarized density islands, particularly those with negative sign, are enhanced obviously and their magnitudes are nearly equal when the number of stubs is large enough. Thereby, the spin conductance at this position drops slowly and finally arrives at zero [see Fig. 2(b)].

In summary, by using the nonequilibrium GF with tight-binding approximation scheme, we have investigated the spin-dependent electron transport in a quantum wire with periodically attached stubs under the modulation of Rashba SOI, where the wire is connected to two normal metal leads. Our results show that a spin-polarized current can be achieved in the output lead due to the longitudinal symmetry of the considered system is broken. Moreover, both the charge and spin-polarized current can be switched on or off by varying the electron energy or the number of stubs. In addition, spin-density islands with high polarization can also be generated inside the periodic stubs. Therefore, the proposed structure has the potential for designing multifunctional semiconductor spintronic devices, such as spin filter, dual charge and spin-polarized current switch as well as spin memory, without using any magnetic materials or applying a magnetic field.

This work was supported by the National Natural Science Foundation of China (Grant Nos. 11264019, 11147156 and 11274108), and by the Research Foundation of Jiangxi Education Department (Grant No. GJJ12532).

[1] N. S. D. D. Awschalom and D. Loss, *Semiconductor Spintronics and Quantum Computation*, (Springer, Berlin) 2002.

[2] I. Žutić, J. Fabian, and S. D. Sarma, Rev. Mod. Phys. **76**, 323 (2004).

[3] J. Fabian, A. Matos-Abiague, C. Ertler, P. Stano, and I. Zutic, Acta Phys. Slov. **57**, 565 (2007).

[4] E. I. Rashba, Sov. Phys. Solid State **2** 1109 (1960); Y. A. Bychkov, E. I. Rashba, J. Phys. C **17**, 6039 (1984).

[5] E. Ya. Sherman, Phys. Rev. B **67**, 161303(R) (2003).

[6] L. E. Golub and E. L. Ivchenko, Phys. Rev. B **69**, 115333 (2004).

[7] G. Engels, J. Lange, T. Schäpers, and H. Lüth, Phys. Rev. B **55**, R1958 (1997).

[8] D. Grundler, Phys. Rev. Lett. **84**, 6074 (2000).

[9] T. Koga, J. Nitta, T. Akazaki, and H. Takayanagi, Phys. Rev. Lett. **89**, 046801 (2002).

[10] L. Saminadayar, C. Bäuerle, and D. Mailly, *Encyclopedia of Nanoscience and Nanotechnology*, (American Scientific, Valencia, CA) 2004.

[11] Z. Y. Zhang, J. Phys: Condens. Matter **19**, 016209 (2007).

[12] F. Zhai and H. Q. Xu, Phys. Rev. B **76**, 035306 (2007).

[13] X. B. Xiao, X. M. Li, and Y. G. Chen, Phys. Lett. A **373**, 4489 (2009).

[14] Y. Ban and E. Y. Sherman, Appl. Phys. Lett. **99**, 112101 (2011).

[15] X. B. Xiao, F. Li, Y. G. Chen and N. H. Liu, Eur. Phys. J. B **85**, 112 (2012).

[16] F. Zhai, K. Chang, and H. Q. Xu, Appl. Phys. Lett. **92**, 102111 (2008).

[17] X. B. Xiao and Y. G. Chen, EPL **90**, 47004 (2010).

[18] X. F. Wang, P. Vasilopoulos, and F. M. Peeters, Phys. Rev. B **65**, 165217 (2002); X. F. Wang and P. Vasilopoulos, Phys. Rev. B **68**, 035305 (2003).

[19] X. F. Wang, Phys. Rev. B **69**, 035302 (2004).

[20] L. B. Zhang, P. Brusheim, and H. Q. Xu, Phys. Rev. B **72**, 045347 (2005).

[21] S. J. Gong and Z. Q. Yang, J. Phys.: Condens. Matter **19**, 446209 (2007).

[22] L. Wang, K. Shen, S. Y. Cho, and M. W. Wu, J. Appl. Phys. 104, 123709 (2009).

[23] G. I. Japaridze, H. Johannesson, and A. Ferraz, Phys. Rev. B **80**, 041308(R) (2009).

[24] M. Malard, I. Grusha, G. I. Japaridze, and H. Johannesson, Phys. Rev. B **84**, 075466 (2011).

[25] G. Thorgilsson, J. Carlos Egues, D. Loss, and S. I. Erlingsson, Phys. Rev. B **85**, 045306 (2012).

[26] L. G. Wang and K. Chang, Solid State Commun. **137**, 260 (2006); L. G. Wang, Kai Chang, and K. S. Chan, J. Appl. Phys. **99**, 043701 (2006).

[27] S. J. Gong and Z. Q. Yang, J. Appl. Phys. **102**, 033706 (2007).

[28] M. Büttiker, Phys. Rev. Lett. **57**, 1761 (1986).

[29] T. P. Pareek and P. Bruno, Phys. Rev. B **63**, 165424 (2001).

[30] P. Brusheim and H. Q. Xu, Phys. Rev. B **74**, 205307 (2006).

[31] A. Yacoby, H. L. Stormer, N. S. Wingreen, K. W. Baldwin, and K. W. West, Phys. Rev. Lett. **77** 4612 (1996); C. T. Liang, M. Pepper, M. Y. Simmons, C. G. Smith, and D. A. Ritchie, Phys. Rev. B **61**, 9952 (2000); R. de Picciotto, L. N. Pfeiffer, K. W. Baldwin, and K. W. West, Phys. Rev. Lett. **92**, 36805 (2004).

[32] K. Nikolić and R. Šordan, Phys. Rev. B **58**, 6555 (1998).